Amplitude Mode in Three-Dimensional Dimerized Antiferromagnets

Yan Qi Qin,[1] B. Normand,[2] Anders W. Sandvik,[3] and Zi Yang Meng[1]
[1]*Beijing National Laboratory for Condensed Matter Physics and Institute of Physics, Chinese Academy of Sciences, Beijing 100190, China*
[2]*Laboratory for Neutron Scattering and Imaging, Paul Scherrer Institute, CH-5232 Villigen PSI, Switzerland*
[3]*Department of Physics, Boston University, 590 Commonwealth Avenue, Boston, Massachusetts 02215, USA*
(Received 17 October 2016; published 6 April 2017)

The amplitude ("Higgs") mode is a ubiquitous collective excitation related to spontaneous breaking of a continuous symmetry. We combine quantum Monte Carlo (QMC) simulations with stochastic analytic continuation to investigate the dynamics of the amplitude mode in a three-dimensional dimerized quantum spin system. We characterize this mode by calculating the spin and dimer spectral functions on both sides of the quantum critical point, finding that both the energies and the intrinsic widths of the excitations satisfy field-theoretical scaling predictions. While the line width of the spin response is close to that observed in neutron scattering experiments on $TlCuCl_3$, the dimer response is significantly broader. Our results demonstrate that highly nontrivial dynamical properties are accessible by modern QMC and analytic continuation methods.

DOI: 10.1103/PhysRevLett.118.147207

The spontaneous breaking of a continuous symmetry allows collective excitations of the direction and amplitude of the order parameter; for O(N) symmetry, there are $N-1$ massless directional (Goldstone) modes and one massive amplitude mode [1–4]. In loose analogy with the standard model, the latter is often called a Higgs mode. A strongly damped amplitude mode has been reported in two dimensions (2D) at the Mott transition of ultracold bosons [5] and at the disorder-driven superconductor-insulator transition [6,7]. In 3D, the amplitude mode is expected on theoretical grounds to be more robust, and indeed the cleanest observation to date of a "Higgs boson" in condensed matter is at the pressure-induced magnetic quantum phase transition (QPT) in the dimerized quantum antiferromagnet $TlCuCl_3$ [8–10].

Below the upper critical number of space-time dimensions, which for an O(N) model is $D_c = 4$, the amplitude mode is unstable, decaying primarily into pairs of Goldstone bosons [11–13]. In both 2D and 3D, the longitudinal dynamic susceptibility exhibits an infrared singularity due to the Goldstone modes [14], whose consequences for the visibility of the amplitude mode have been investigated extensively in 2D [15–17]. It was noted [14] that the scalar O(N)-symmetric susceptibility remains uncontaminated by infrared contributions, which should permit the amplitude mode to be observed as a well-defined peak. The $(3+1)$D O(3) case of $TlCuCl_3$ is at D_c and the amplitude mode is critically damped, meaning that its width is proportional to its energy at the mean-field level [9,18–20]. This mode can be probed through the spin response (longitudinal susceptibility) by neutron spectroscopy, and measurements over a wide range of pressures reveal a rather narrow peak width of just 15% of the excitation energy [10]. The value of this near-constant width-to-energy ratio is the key to the mode visibility, thus calling for unbiased numerical calculations in suitable model Hamiltonians.

In this Letter, we provide a systematic investigation of the dynamics and scaling of the amplitude mode at coupling values across the QPT in a 3D dimerized spin-1/2 antiferromagnet, by performing large-scale stochastic series expansion quantum Monte Carlo (SSE-QMC) simulations and applying advanced stochastic analytic-continuation (SAC) methods. Thus we provide an unbiased numerical demonstration that the amplitude mode is critically damped and that its energy, width, and height obey field-theoretical predictions. Beyond these universal scaling forms, we quantify the nonuniversal width-to-energy ratios of the amplitude-mode peaks in the spin and dimer channels.

We consider the double-cubic geometry shown in Fig. 1 [21], which consists of two simple cubic lattices whose sites are connected pairwise by nearest-neighbor Heisenberg exchange interactions, $J_{ij}\vec{S}_i \cdot \vec{S}_j$, with $J_{ij} = J$ in each cubic lattice and $J_{ij} = J'$ for inter-cube (dimer) bonds. Increasing the ratio $g = J'/J$ drives a QPT where the ground state changes from a "renormalized classical" [22,23] antiferromagnetic (AFM) state to a quantum disordered (QD) dimer-singlet state (Fig. 1). This transition is in the same universality class as the pressure-driven QPT in $TlCuCl_3$. In a recent QMC analysis of the static properties of the double-cubic system [24], we established the quantum critical point (QCP) as $g_c = 4.837\,04(6)$ and quantified the logarithmic (log) scaling corrections expected near criticality in the AFM state at D_c.

We use SSE-QMC [25,26] simulations to measure both spin and dimer correlation functions in imaginary time; technical details may be found in Sec. SI of the

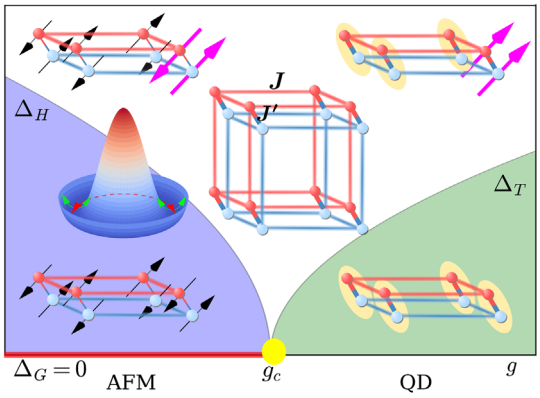

FIG. 1. Schematic representation of ground states, excitation processes, and corresponding gaps in a dimerized antiferromagnet. The ratio $g = J'/J$ of the intra- and interdimer coupling constants controls a QPT from an AFM to a QD state. In the AFM phase, the excitations are two gapless spin waves (Goldstone modes, $\Delta_G = 0$, red line) plus an amplitude mode with gap Δ_H, corresponding respectively to axial and radial fluctuations in the "Mexican hat" potential. In the QD phase, singlet-triplet dimer excitations have gap Δ_T.

Supplemental Material (SM) [27]. The former probes $S = 1$ excitations of the ground state and contains the longitudinal susceptibility, while the latter, the symmetric scalar response [14–16], probes $S = 0$ excitations. We employ SAC methods [32–37] to obtain high-resolution data for the spin and dimer spectral functions, and discuss the concepts and practicalities of this procedure in Sec. SII of the SM [27]. Depending on the value of g, both spectral functions contain features arising from the Goldstone, amplitude, and triplon (gapped singlet-triplet) excitations. Henceforth we use the term "Higgs" as shorthand for the amplitude-mode contributions. The nature and energies of these modes are represented schematically in Fig. 1.

Our simulations are performed on a system of $N = 2L^3$ sites at an inverse temperature $J\beta = 2L$, such that the low-temperature limit, $T \to 0$, is achieved as $L \to \infty$. The dynamical magnetic ($S = 1$) response is obtained from the spin correlation function

$$S(\mathbf{q}, \tau) = \langle S^z_{-\mathbf{q}}(\tau) S^z_{\mathbf{q}}(0) \rangle, \tag{1}$$

where τ is the imaginary time [Eq. (S1)] and

$$S^z_{\mathbf{q}} = \frac{1}{\sqrt{N}} \sum_{\mathbf{r}} e^{-i\mathbf{q}\cdot\mathbf{r}} (S^{1z}_r - S^{2z}_r), \tag{2}$$

where superscripts 1 and 2 denote the two cubic lattices. When analytically continued to real frequency, $S(\mathbf{q}, \tau)$ gives the dynamical structure factor, $S(\mathbf{q}, \omega)$, measured by inelastic neutron scattering. Our simulations contain no breaking of spin-rotation symmetry and thus do not separate the longitudinal and transverse components of $S(\mathbf{q}, \omega)$ explicitly. The Higgs mode of the AFM phase is contained in the longitudinal part, but the transverse part contains both spin-wave excitations and a multimagnon continuum that could obscure the Higgs contribution in the rotationally averaged $S(\mathbf{q}, \omega)$. However, unlike the 2D case [38], the transverse continuum is expected to be very small in 3D, especially at the staggered wave vector, $\mathbf{q} = \mathbf{Q} = (\pi, \pi, \pi)$, on which we focus here.

The scalar ($S = 0$) dynamical response is obtained from the dimer correlation function at the zone center, $\mathbf{q} = \mathbf{\Gamma} = (0, 0, 0)$, which is given by

$$D(\mathbf{\Gamma}, \tau) = \langle B_\Gamma(\tau) B_\Gamma(0) \rangle, \qquad B_\Gamma = \frac{1}{\sqrt{N}} \sum_r B_r, \tag{3}$$

where $B_r = \mathbf{S}^1_r \cdot \mathbf{S}^2_r - \langle \mathbf{S}^1_r \cdot \mathbf{S}^2_r \rangle$ is the inter-cubic dimer bond operator. This quantity was also employed in a recent study of the $(2+1)$D (bilayer) model [39]. The real-frequency quantity $D(\mathbf{\Gamma}, \omega)$ may be probed experimentally by Raman scattering [40,41].

Gap information can also be extracted by a direct analysis of the large-τ decay of the correlation functions [42,43]. Considering the spin sector, the smallest singlet-triplet gap occurs at $\mathbf{q} = \mathbf{Q}$ and in the QD phase $S(\mathbf{Q}, \tau)$ is dominated by the triplon mode. In the AFM phase, this gap corresponds to the lowest Goldstone mode, which has only a finite-size energy proportional to $1/N$. Thus $S(\mathbf{Q}, \tau)$ decays very slowly with τ in this case and the dominant Goldstone contribution threatens to obscure the Higgs contribution [14–17,44]. Examples of imaginary-time data for $S(\mathbf{Q}, \tau)$ and of gap extractions are presented in Secs. SII and SIII of the SM [27].

We begin the discussion of our results by analyzing the triplon gap in the QD phase ($g > g_c$). For a given value of g, we extract the finite-size gap, $\Delta_T(L)$, from $S(\mathbf{Q}, \tau)$ for a range of system sizes. As shown in Fig. 2(a), $\Delta_T(L)$ decreases with increasing L before converging to the thermodynamic limit. The extrapolated values of $\Delta_T(g)$ are shown in Fig. 2(b) as a function of the separation $(|g - g_c|/g_c)$ from the QCP.

In the ϕ^4 theory for an O(N) order parameter, at $D = D_c$ one expects physical quantities to exhibit power-law scaling with mean-field critical exponents, but with multiplicative log corrections [3,45], which have now been found in a number of recent studies [24,46,47]. The scaling form of the triplon gap can be obtained directly from the correlation length ($\Delta \sim 1/\xi$), whence

$$\Delta_T \sim (|g - g_c|/g_c)^\nu \ln^{-\hat{\nu}}(|g - g_c|/g_c), \tag{4}$$

with $\nu = 1/2$ [3,48] and $\hat{\nu} = (N+2)/2(N+8)$ from perturbative renormalization-group calculations [45,49], i.e., $\hat{\nu} = 5/22 \approx 0.227$ for $N = 3$. It is clear from Fig. 2(b) that Eq. (4) describes the data far better than the pure mean-field form and, by performing an optimized fit [24] with $\hat{\nu}$ as a free parameter, we deduce the exponent $\hat{\nu} = 0.230(2)$, fully consistent with the theoretical prediction.

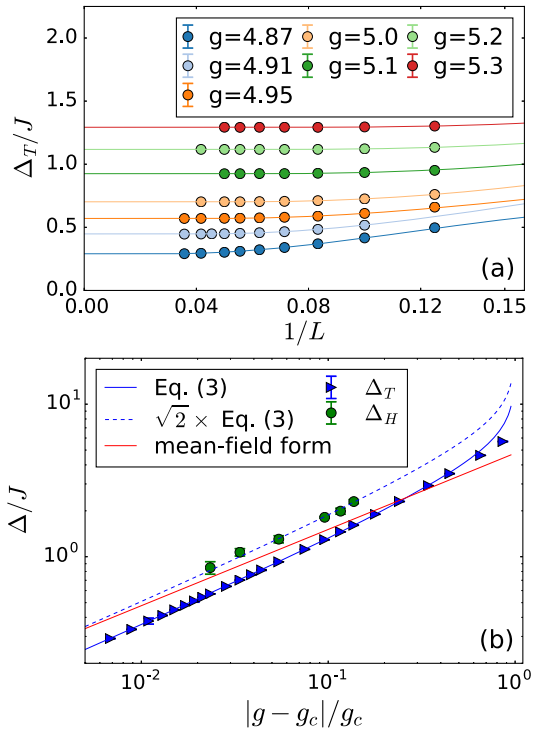

FIG. 2. (a) Extrapolation of finite-size triplon gaps, using the form $\Delta_T(L) = a\exp(-bL) + c$, shown for selected values of $g > g_c$ (QD phase). (b) Triplon gaps in the thermodynamic limit (blue triangles), shown as a function of $|g - g_c|/g_c$. The red line is a pure mean-field (square-root) form, the blue line includes the log correction of Eq. (4) with fitted exponent $\hat{\nu} = 0.230(2)$, and green points show the extrapolated Higgs energy, Δ_H, obtained for values of $g < g_c$ (AFM phase) mirroring those used in panel (a). The blue dashed line is the log-corrected Δ_T result multiplied by $\sqrt{2}$. Error bars in both panels are smaller than the symbol sizes.

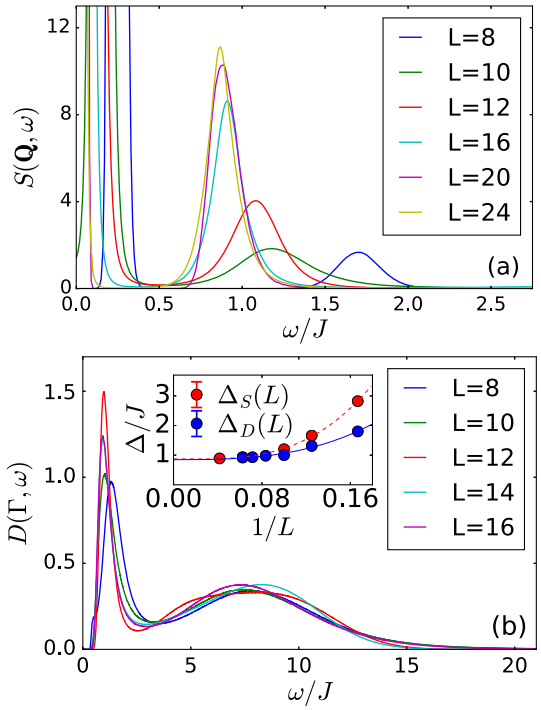

FIG. 3. (a) $S(\mathbf{Q},\omega)$ and (b) $D(\mathbf{\Gamma},\omega)$ obtained by SAC at $g = 4.724$ for different system sizes. The large low-energy (Goldstone) peak in panel (a) is cut off in order to show the secondary (Higgs) peak. The lower peak in panel (b) is the Higgs mode. The positions of both Higgs contributions converge with increasing L to the same thermodynamic limit, as shown in the inset of panel (b). Spectral features outside the energy ranges shown are extremely weak.

To study the amplitude mode in detail, we analyze the spectral functions $S(\mathbf{Q},\omega)$ and $D(\mathbf{\Gamma},\omega)$ in the AFM phase ($g < g_c$) near g_c. Figure 3 shows both quantities at $g = 4.724$ for several system sizes. Because SSE-QMC calculations of $D(\mathbf{\Gamma},\tau)$ are significantly more demanding (Sec. SI), these are restricted to $L \leq 16$, whereas for $S(\mathbf{Q},\tau)$ we access sizes up to $L = 24$.

$S(\mathbf{Q},\omega)$ [Fig. 3(a)] is dominated by the Goldstone contribution, whose energy (spectral weight) is proportional to $1/N$ (N) at $T = 0$ (becoming the magnetic Bragg peak as $L \to \infty$). The Higgs spectral weight also diverges as $g \to g_c$; away from g_c the Higgs mode remains as a clearly resolved finite-energy peak with convergent spectral weight, as also observed experimentally in $TlCuCl_3$ [9,10]. In $D(\mathbf{\Gamma},\omega)$ [Fig. 3(b)], the Higgs contribution is the distinctive low-energy peak. It is separated by a region of suppressed spectral weight from a broad maximum at higher energies due to multiple excitations. At low energies, one expects a characteristic scaling form on which we comment in detail below.

We observe good convergence with increasing L in each of $S(\mathbf{Q},\omega)$ and $D(\mathbf{\Gamma},\omega)$. The peak widths in both quantities are invariant on increasing the amount of QMC data, demonstrating that any artificial broadening arising from the SAC procedure is negligible. Examples of supporting tests are presented in Sec. SII of the SM [27]. We have confirmed by a bootstrapping analysis that the fluctuations in the height and width of the lower $D(\mathbf{\Gamma},\tau)$ peak for $L \geq 10$ in Fig. 3(b) reflect statistical errors. Our system sizes are sufficient for a reliable study of the $L \to \infty$ limit in both sectors for the g values shown in Fig. 3 (i.e., $g \approx g_c - 0.1$).

We find that the positions of the finite-energy peaks in $S(\mathbf{Q},\tau)$ and $D(\mathbf{\Gamma},\tau)$ converge to the same value as $L \to \infty$ [inset, Fig. 3(b)]. In the phenomenological U(1) model for the broken-symmetry phase, one expects the $S = 0$ Higgs mode to be an elementary scalar [50], and thus in the AFM phase that the Higgs part of the $S = 1$ spectrum arises from a combination of this scalar with a gapless spin wave ($S = 1$, $\mathbf{q} = \pm\mathbf{Q}$). Although our finite-size calculations contain no explicit symmetry-breaking, they reflect this physics directly in that the spin peak lies higher than the dimer peak and their energy difference scales with $1/N$, as expected for a Goldstone mode. Thus the consistency between peaks in the $S = 0$ and 1 spectral functions

provides strong confirmation that both do indeed correspond to the Higgs mode.

In Fig. 2(b) we compare the extrapolated Higgs energies in the AFM phase with the triplet gaps in the QD phase at the same distance, $|g-g_c|/g_c$, from the QCP. The predicted $\sqrt{2}$ ratio [44,46,48] between Δ_H and Δ_T is clearly obeyed over this rather broad coupling range. We stress that this relation implies the presence of equivalent multiplicative log corrections [Eq. (4)] to both Δ_T in the QD phase and Δ_H on the AFM side.

To investigate the scaling properties of the spectral functions near the QCP, we normalize ω by the $L\to\infty$ Higgs gap; results for $\Delta_H^2 S(\mathbf{Q},\omega/\Delta_H)$ and $D(\mathbf{\Gamma},\omega/\Delta_H)$ are shown respectively in Figs. 4(a) and 4(b) for the largest accessible system sizes. The amplitude-mode contributions to both the spin and dimer spectral functions exhibit near-ideal data collapse when scaled in this way. The collapse of the peak positions indicates that our data represent the quantum critical regime and the thermodynamic limit. The collapse of the peak widths demonstrates the critically damped nature of the Higgs mode. We note that Fig. 4(a) also indicates the spectral weight of the next-order $S=1$ processes, whose peak positions near $\omega=2\Delta_H$ suggest excitations involving two Higgs modes, but statistical errors preclude a deeper analysis.

A universal scaling form for the scalar susceptibility (dimer spectral function) in the vicinity of the QCP,

$$D(\mathbf{\Gamma},\omega)\sim\Delta_H^{d+z-2/\nu}\Phi(\omega/\Delta_H), \tag{5}$$

has been derived perturbatively in $1/N$ for the $O(N)$ model [15–17] and by a $4-\epsilon$ expansion [44]. In $(3+1)$D with $z=1$, one expects $D(\mathbf{\Gamma},\omega)=\Phi(\omega/\Delta_H)$, which is fully consistent with the data in Fig. 4(b). This type of scaling has been documented in $(2+1)$D for both O(2) [16,17,51–53] and O(3) models [39,53], but Fig. 4(b) constitutes the only unbiased numerical demonstration to date in $(3+1)$D. The infrared tail is expected [14] to have the scaling form $D(\mathbf{\Gamma},\omega)\propto\omega^4$, but with the available system sizes is too weak to verify this. For $S(\mathbf{Q},\omega/\Delta_H)$, we obtain data collapse by appealing to the result [9] that the integrated spectral weight diverges as $1/\Delta_H$ when $g\to g_c$, which requires a rescaling by Δ_H^2 [Fig. 4(a)].

The scaling function $\Phi(\omega/\Delta_H)$ is shown in Ref. [44] to approach a δ-function at $g=g_c$, due to the presence of log corrections in the width-to-energy ratios [18,19]. For a quantitative analysis of the Higgs-peak widths, in Fig. 4(c) we show the size-dependence of the ratios obtained from the FWHM σ_S of the spin and σ_D of the dimer peak. The error bars obtained by bootstrapping are significant, but it is clear that (i) the L-dependence of σ_S/Δ_H and σ_D/Δ_H is weak, (ii) any g-dependence is weak, and (iii) σ_D exceeds σ_S by a factor of 3. We fit error-weighted averages of the width ratios, obtained from all g values at each L, to a quadratic polynomial in $1/L$, as shown in Fig. 4(c). At the

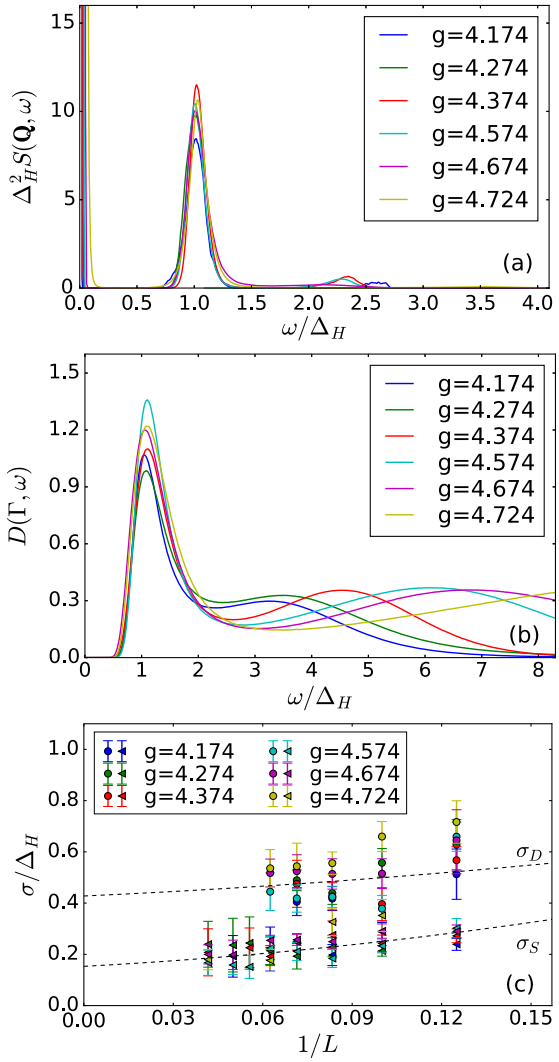

FIG. 4. (a) Scaled spectrum, $\Delta_H^2 S(\mathbf{Q},\omega/\Delta_H)$, calculated with $L=24$ for a range of g values. (b) $D(\mathbf{\Gamma},\omega/\Delta_H)$ calculated with $L=16$. (c) Width-to-energy ratios shown as functions of $1/L$. Circles and triangles are obtained respectively from $D(\mathbf{\Gamma},\omega/\Delta_H)$ and $S(\mathbf{Q},\omega/\Delta_H)$. Dashed lines are second-order polynomial fits to error-weighted average ratios.

mean-field level, we estimate the constant ratios $\sigma_S/\Delta_H=0.15(4)$ and $\sigma_D/\Delta_H=0.43(6)$. The log dependence on $|g-g_c|$ is too weak to discern given the quality of the present data and the separation from the critical point. However, future calculations with smaller $|g-g_c|$, larger system sizes, and higher precision in $G(\tau)$ and $D(\tau)$ should be able to detect log corrections also in the width-to-energy ratios.

Remarkably, our SAC value for σ_S/Δ_H on the double-cubic lattice is in excellent agreement with the neutron scattering results for $TlCuCl_3$ near its QCP [9,10,20]. Given the difference in lattices and couplings, this result mandates a deeper investigation of possible reasons for a very weak dependence on microscopic details. The significantly larger value of σ_D/Δ_H reflects the different

states probed by the two spectral functions, namely the elementary Higgs ($S = 0$) and combined Higgs-Goldstone ($S = 1$) excitations. This also implies different matrix-element effects in the peak shapes, which are evident in the different scaling forms of the peak areas in Fig. 4.

In summary, we have used large-scale quantum Monte Carlo simulations to investigate the quantum critical dynamics of the amplitude (Higgs) mode in a 3D dimerized antiferromagnet. Our work demonstrates that modern SAC methods are capable of resolving complex spectral functions, here with two peaks and nontrivial scaling behavior of both the peak widths and heights. Our results not only verify the scaling predictions based on field-theory methods but also provide line-width information and nonuniversal factors that lie beyond current analytical treatments. The type of calculations reported here can be performed for different momenta, to study the dispersion of the amplitude mode and the evolution of its width in the spin and dimer sectors, as well as for the lattice geometry and exchange couplings of $TlCuCl_3$.

We thank Stefan Wessel for communicating the results of a related investigation [54] recently, Hui Shao for collaborations on the SAC method, and Oleg Sushkov for discussions. Numerical calculations were performed on the Tianhe-1A platform at the National Supercomputer Center in Tianjin. Y. Q. Q. and Z. Y. M. acknowledge support from the Ministry of Science and Technology of China under Grant No. 2016YFA0300502, the National Science Foundation of China under Grants No. 11421092 and No. 11574359, and the National Thousand-Young-Talents Program of China. Y. Q. Q. would like to thank the Condensed Matter Theory Visitors Program of Boston University. A. W. S. was supported by the NSF under Grant No. DMR-1410126 and would also like to thank the Institute of Physics of the Chinese Academy of Sciences for visitor support.

[1] J. Goldstone, A. Salam, and S. Weinberg, Phys. Rev. **127**, 965 (1962).
[2] P. W. Higgs, Phys. Rev. Lett. **13**, 508 (1964).
[3] J. Zinn-Justin, *Quantum Field Theory and Critical Phenomena* (Clarendon Press, Oxford, 2002).
[4] S. Sachdev, *Quantum Phase Transitions* (Cambridge University Press, Cambridge, 2011).
[5] M. Endres, T. Fukuhara, D. Pekker, M. Cheneau, P. Schauss, C. Gross, E. Demler, S. Kuhr, and I. Bloch, Nature (London) **487**, 454 (2012).
[6] M. Swanson, Y. L. Loh, M. Randeria, and N. Trivedi, Phys. Rev. X **4**, 021007 (2014).
[7] D. Sherman, U. S. Pracht, B. Gorshunov, S. Poran, J. Jesudasan, M. Chand, P. Raychaudhuri, M. Swanson, N. Trivedi, A. Auerbach, M. Scheffler, A. Frydman, and M. Dressel, Nat. Phys. **11**, 188 (2015).
[8] C. Rüegg, A. Furrer, D. Sheptyakov, T. Strässle, K. W. Krämer, H.-U. Güdel, and L. Mélési, Phys. Rev. Lett. **93**, 257201 (2004).
[9] C. Rüegg, B. Normand, M. Matsumoto, A. Furrer, D. F. McMorrow, K. W. Krämer, H. U. Güdel, S. N. Gvasaliya, H. Mutka, and M. Boehm, Phys. Rev. Lett. **100**, 205701 (2008).
[10] P. Merchant, B. Normand, K. W. Kramer, M. Boehm, D. F. McMorrow, and C. Ruegg, Nat. Phys. **10**, 373 (2014).
[11] S. Sachdev, Phys. Rev. B **59**, 14054 (1999).
[12] W. Zwerger, Phys. Rev. Lett. **92**, 027203 (2004).
[13] N. Dupuis, Phys. Rev. E **83**, 031120 (2011).
[14] D. Podolsky, A. Auerbach, and D. P. Arovas, Phys. Rev. B **84**, 174522 (2011).
[15] D. Podolsky and S. Sachdev, Phys. Rev. B **86**, 054508 (2012).
[16] S. Gazit, D. Podolsky, and A. Auerbach, Phys. Rev. Lett. **110**, 140401 (2013).
[17] S. Gazit, D. Podolsky, A. Auerbach, and D. P. Arovas, Phys. Rev. B **88**, 235108 (2013).
[18] I. Affleck, Phys. Rev. Lett. **62**, 474 (1989).
[19] I. Affleck and G. F. Wellman, Phys. Rev. B **46**, 8934 (1992).
[20] Y. Kulik and O. P. Sushkov, Phys. Rev. B **84**, 134418 (2011).
[21] S. Jin and A. W. Sandvik, Phys. Rev. B **85**, 020409 (2012).
[22] S. Chakravarty, B. I. Halperin, and D. R. Nelson, Phys. Rev. B **39**, 2344 (1989).
[23] A. V. Chubukov, S. Sachdev, and J. Ye, Phys. Rev. B **49**, 11919 (1994).
[24] Y. Q. Qin, B. Normand, A. W. Sandvik, and Z. Y. Meng, Phys. Rev. B **92**, 214401 (2015).
[25] A. W. Sandvik, Phys. Rev. B **59**, R14157 (1999).
[26] O. F. Syljuåsen and A. W. Sandvik, Phys. Rev. E **66**, 046701 (2002).
[27] For details see the Supplemental Material at http://link.aps.org/supplemental/10.1103/PhysRevLett.118.147207, which contains Refs. [28–31].
[28] A. W. Sandvik and J. Kurkijärvi, Phys. Rev. B **43**, 5950 (1991).
[29] A. W. Sandvik, J. Phys. A **25**, 3667 (1992).
[30] M. Jarrell and J. Gubernatis, Phys. Rep. **269**, 133 (1996).
[31] D. Bergeron and A.-M. S. Tremblay, Phys. Rev. E **94**, 023303 (2016).
[32] A. W. Sandvik, Phys. Rev. B **57**, 10287 (1998).
[33] K. S. D. Beach, arXiv:cond-mat/0403055.
[34] O. F. Syljuåsen, Phys. Rev. B **78**, 174429 (2008).
[35] S. Fuchs, T. Pruschke, and M. Jarrell, Phys. Rev. E **81**, 056701 (2010).
[36] A. W. Sandvik, Phys. Rev. E **94**, 063308 (2016).
[37] H. Shao and A. W. Sandvik (unpublished).
[38] A. W. Sandvik and R. R. P. Singh, Phys. Rev. Lett. **86**, 528 (2001).
[39] M. Lohöfer, T. Coletta, D. G. Joshi, F. F. Assaad, M. Vojta, S. Wessel, and F. Mila, Phys. Rev. B **92**, 245137 (2015).
[40] P. A. Fleury and R. Loudon, Phys. Rev. **166**, 514 (1968).

[41] B. S. Shastry and B. I. Shraiman, Phys. Rev. Lett. **65**, 1068 (1990).
[42] A. Sen, H. Suwa, and A. W. Sandvik, Phys. Rev. B **92**, 195145 (2015).
[43] H. Suwa, A. Sen, and A. W. Sandvik, Phys. Rev. B **94**, 144416 (2016).
[44] Y. T. Katan and D. Podolsky, Phys. Rev. B **91**, 075132 (2015).
[45] R. Kenna, Nucl. Phys. **B691**, 292 (2004).
[46] H. D. Scammell and O. P. Sushkov, Phys. Rev. B **92**, 220401 (2015).
[47] D.-R. Tan and F.-J. Jiang, Phys. Rev. B **95**, 054435 (2017).
[48] S. Sachdev, arXiv:0901.4103.
[49] R. Kenna, in *Order, Disorder and Criticality*, edited by Y. Holovatch (World Scientific, Singapore, 2012), Vol. III.
[50] D. Pekker and C. M. Varma, Annu. Rev. Condens. Matter Phys. **6**, 269 (2015).
[51] L. Pollet and N. Prokof'ev, Phys. Rev. Lett. **109**, 010401 (2012).
[52] K. Chen, L. Liu, Y. Deng, L. Pollet, and N. Prokof'ev, Phys. Rev. Lett. **110**, 170403 (2013).
[53] F. Rose, F. Léonard, and N. Dupuis, Phys. Rev. B **91**, 224501 (2015).
[54] M. Lohöfer and S. Wessel, preceding Letter, Phys. Rev. Lett. **118**, 147206 (2017).